

# Structure determination of the $(3\sqrt{3} \times 3\sqrt{3})$ reconstructed $\alpha\text{-Al}_2\text{O}_3(0001)$

Igor Vilfan <sup>a,b</sup>, Thierry Deutsch <sup>a</sup>, Frédéric Lançon <sup>a</sup>, Gilles Renaud <sup>a</sup>

<sup>a</sup>*Département de Recherche Fondamentale sur la Matière Condensée, CEA-Grenoble,  
F-38054 Grenoble cedex 9, France*

<sup>b</sup>*J. Stefan Institute, P.O. Box 3000, SI-1001 Ljubljana, Slovenia*<sup>1</sup>

---

## Abstract

Grazing-incidence X-ray diffraction data are combined with energy-minimization calculations to analyse the atomic structure of the Al-rich  $(3\sqrt{3} \times 3\sqrt{3})R30^\circ$  reconstructed surface of sapphire  $\alpha\text{-Al}_2\text{O}_3(0001)$ . The experiments on the BM32 beamline of the ESRF provide the non-integer-order diffraction intensities and, after Fourier transform, an incomplete Patterson map. The computer simulations are implemented to obtain structural information from this map. In the simulations, the interactions between the Al overlayer atoms were described with the Sutton-Chen potential and the interactions between the overlayer and the sapphire substrate with a laterally modulated Lennard-Jones potential. We have shown that the hexagonal reconstructed unit cell is composed of triangles where the two layers of Al adatoms are FCC(111) ordered whereas between the triangles the stacking is FCC(001).

*Key words:* Surface relaxation and reconstruction, Sapphire, Al thin films, X-ray scattering, computer simulations.

*PACS:* 68.35.Bs, 61.10.Eq, 68.55.Jk, 02.70.Ns

---

## 1 Introduction

The (0001) surface of sapphire  $\alpha\text{-Al}_2\text{O}_3$  is, because of its insulating character, an important substrate for very high frequency microelectronic devices. Therefore it is of crucial importance to understand the stability and structure of this surface at high temperatures. In equilibrium at room temperature, a clean (0001) surface is unreconstructed and is terminated with a single Al layer on top of the last oxygen layer [1–3]. Upon heating up to  $\sim 1500$  C in ultra-high vacuum (UHV), oxygen

---

<sup>1</sup> Permanent address of the corresponding author.

evaporates from the crystal, leaving an Al rich and reconstructed surface behind it [4]. Al atoms that are left on the sapphire surface are responsible for a sequence of surface reconstructions:  $(\sqrt{3} \times \sqrt{3})\text{R}30^\circ$  when sapphire is heated to about 1100 C,  $(2\sqrt{3} \times 2\sqrt{3})\text{R}30^\circ$  at 1150 C,  $(3\sqrt{3} \times 3\sqrt{3})\text{R}30^\circ$  at 1250 C and finally  $(\sqrt{31} \times \sqrt{31})\text{R}\pm 9^\circ$  structure at 1350 C [5]. So far only the structure of the most stable, i.e., of the  $(\sqrt{31} \times \sqrt{31})\text{R}\pm 9^\circ$  reconstruction has been satisfactorily determined [6,7]. Very recently, this structure has also been investigated by Barth and Reichling with the atomic-scale-resolution scanning force microscope [8]. No information on the real-space structures of other reconstructions is available so far.

In this letter we concentrate on the  $(3\sqrt{3} \times 3\sqrt{3})\text{R}30^\circ$  reconstruction of the sapphire (0001) surface. Although this is a transient reconstruction, it was prepared in a very well defined state with large domain sizes [5,9].

Our analysis is based on grazing-incidence X-ray diffraction (GIXD) data where some surface diffraction intensities are hidden in the bulk Bragg peaks and the corresponding Patterson map is incomplete [10]. To obtain the real-space structure, therefore, we combined the Patterson map with computer simulations using semi-empirical potentials.

## 2 Experiment

The structure was investigated experimentally by grazing-incidence X-ray diffraction using the SUV set-up [11] of the BM32 beamline at the ESRF. This is equipped with a large UHV chamber ( $3 \times 10^{-11}$  mbar base pressure) with RHEED, AES, mass analyser, a high temperature (up to 1500 C) furnace and several deposition sources. The sample was prepared by heating at 1250 C for 20 min, which yielded a  $(3\sqrt{3} \times 3\sqrt{3})$  reconstruction of very high quality, as checked by *in situ* RHEED, and negligible segregation of contaminants, as checked by AES. A 18 keV doubly focused monochromatic X-ray beam was used, with a  $0.2(\text{H}) \times 0.2(\text{V}) \text{ mm}^2$  size and  $0.5(\text{H}) \times 0.1(\text{V}) \text{ mrad}^2$  convergence at the vertical sample location. The angular acceptance of the NaI detector was set to  $20(\text{H}) \times 4(\text{V}) \text{ mrad}^2$ . The incident angle was fixed at the critical angle for total external reflection during the whole measurement. A total of 1790 in-plane reflections were measured, showing  $p6mm$  symmetry. These were integrated over azimuthal rotation and corrected for background, effective area, polarisation and Lorentz factors [12] to extract the in-plane structure-factor amplitudes  $F_{hk0}$ . This reduced to 240 inequivalent peaks. The experimental diffraction pattern in  $1/6$  of the reciprocal space is shown as right-hand semi-circles in Fig. 1, with their radii proportional to  $F_{hk0}$ . The  $h$  and  $k$  indices are in reciprocal lattice units of the  $(3\sqrt{3} \times 3\sqrt{3})\text{R}30^\circ$  surface reconstruction. Since the phases of  $F_{hk0}$  are unknown, we cannot directly determine the real-space density distribution. In addition, the amplitudes at the bulk Bragg reflections are unknown since the contribution of the surface reconstruction is hidden in the bulk contribu-

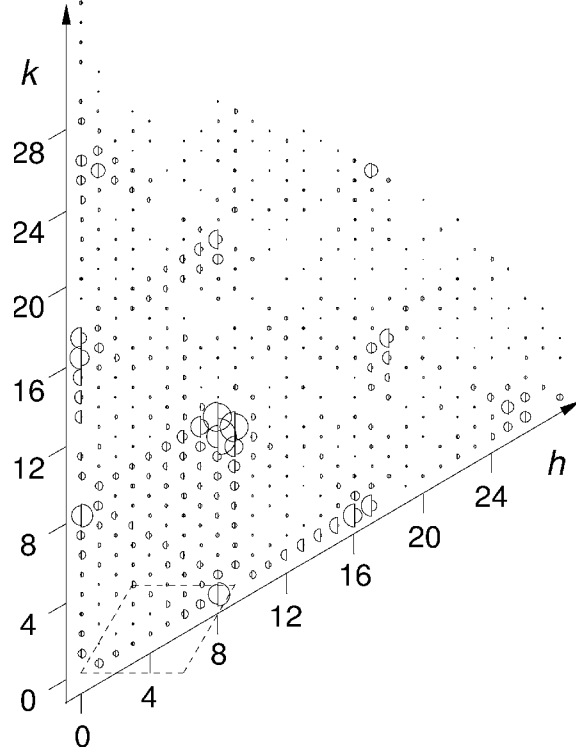


Fig. 1. Diffraction pattern of the  $(3\sqrt{3} \times 3\sqrt{3})R30^\circ$  reconstructed surface of sapphire (0001). The areas of semi-circles are proportional to the intensity of diffraction spots. The right-hand semi-circles are experimental results and the left-hand ones correspond to the structure proposed in this paper. The in-plane bulk reflections are omitted from the graph. The dashed lines show the unreconstructed reciprocal cell.

tion. Therefore the Fourier transform of the experimental  $F_{hk0}^2$  gives an incomplete Patterson map, i.e., an incomplete electron (atom) density-density correlation function. The incomplete Patterson map of the  $(3\sqrt{3} \times 3\sqrt{3})R30^\circ$  reconstructed sapphire (0001) is shown in Fig. 2(a).

### 3 Simulations

Although the Patterson map does not give the real-space structure, it is the starting point to build the real-space models. It tells us that the surface atoms that contribute to the more compact regions of the Patterson map are ordered on a hexagonal lattice, very similar to the “ordered domains” seen also in the  $(\sqrt{31} \times \sqrt{31})R\pm 9^\circ$  reconstruction of sapphire [6,7]. Therefore we constructed the overlayer assuming that sapphire is covered by two FCC(111) layers of Al with the nearest-neighbour separation  $\sim 4\%$  larger than the corresponding sapphire spacing. The lattice misfit inevitably leads to perturbations in the close-packed FCC(111) structure, creating a commensurate structure composed of “domains”, where the overlayer atoms have perfect FCC(111) or hexagonal close-packed ordering, separated by a kind of “do-

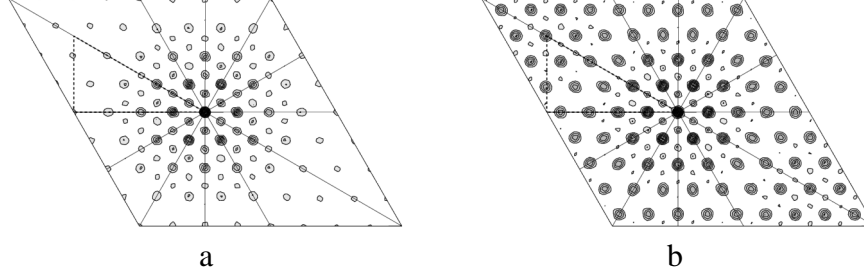


Fig. 2. The Patterson map of one reconstructed unit cell on sapphire. (a) Incomplete Patterson map based on the experimental diffraction data only, (b) Patterson map when the intensities calculated from the model at the in-plane bulk reflections are added to the experimental diffraction data.

main walls”. Whereas the atomic structure in the domain walls is disordered in the  $(\sqrt{31} \times \sqrt{31})$  reconstruction [6–8], the Patterson map of the  $(3\sqrt{3} \times 3\sqrt{3})$  reconstruction in Fig. 2 suggests a much more ordered structure of domain walls. We generated several initial structures with hexagonal close-packed atom ordering in the domains with domain walls between them.

Such reconstructions are too large to be investigated with *ab initio* methods. Therefore we described the interactions between the Al overlayer atoms with the semi-empirical Sutton–Chen potential [13,14] and the effect of the substrate on the overlayer with a phenomenological potential field with hexagonal symmetry. The energy minimization was described in detail in [7].

The semi-empirical many-body Sutton-Chen potential

$$U_{\text{SC}} = \frac{1}{2} \sum_{i \neq j} \epsilon \left( \frac{a}{r_{ij}} \right)^n - \epsilon C \sum_i \sqrt{\rho_i} \quad (1)$$

includes the core repulsion potential (first term) and the bonding energy mediated by the electrons (second term).  $r_{ij}$  is the separation between the atoms  $i$  and  $j$ ,  $\rho_i$  is an effective local electron density at the site  $i$ :

$$\rho_i = \sum_{j \neq i} \left( \frac{a}{r_{ij}} \right)^m \quad (2)$$

and  $a$  is the lattice constant of an Al FCC crystal.  $\epsilon$  and  $C$  are parameters of the model which, together with the exponents  $n$  and  $m$ , determine the repulsive and cohesive energies, respectively. We used the following values for the potential parameters of Al [13]:

$$m = 6, \quad n = 7, \quad \epsilon = 33.147 \text{ meV}, \quad C = 16.399.$$

The potential was truncated continuously (with a fifth order polynomial) between

$r/r_0 = 3.17$  and  $3.32$  ( $r_0$  is the nearest-neighbour distance). In this way the interaction with 68 neighbours would be included if Al were perfectly ordered in two FCC(111) planes.

In general, the overlayers or adatoms are weakly bound to the substrate and well separated from it [15]. In addition, the substrate is much stiffer than the Al overlayer, therefore the relaxation of the substrate caused by the overlayer was neglected in the simulations. The substrate potential was expanded in a power series and only the six lowest-order terms were retained [7],

$$U_S = U_{LJ}(z) \frac{U_L - \cos(\vec{k}_1 \cdot \vec{r}) \cos(\vec{k}_2 \cdot \vec{r}) \cos(\vec{k}_3 \cdot \vec{r})}{U_L - 1} \quad (3)$$

where

$$\vec{k}_1 = \frac{2\pi}{a_s}(0, 1), \quad \vec{k}_2 = \frac{\pi}{a_s}(\sqrt{3}, -1), \quad \vec{k}_3 = \frac{\pi}{a_s}(-\sqrt{3}, -1) \quad (4)$$

are the unit vectors in the plane of the surface and  $a_s$  the substrate lattice constant. The parameter  $U_L$  controls the strength of the lateral modulation of the potential, and  $U_{LJ}$ ,

$$U_{LJ}(z) = U_0 \left[ \left( \frac{z_0}{z} \right)^9 - 2 \left( \frac{z_0}{z} \right)^3 \right], \quad (5)$$

its  $z$ -dependence, in the direction perpendicular to the surface. Expression (5) is the Lennard-Jones potential integrated over the semi-infinite substrate where  $U_0$  is the depth of the substrate potential and  $z_0$  determines the position of the minimum and the width of the potential in the vertical direction. The potential has six equally deep minima in the surface unit cell, to accommodate three overlayer atoms in each monolayer. Thus, the overlayer-substrate potential is described by three *variational parameters*:  $U_L$ ,  $U_0$  and  $z_0$ .

The parameters  $U_L$ ,  $U_0$  and  $z_0$  were varied to minimize the difference between the experimental and calculated structure factors [5]:

$$\chi^2 = \frac{1}{N} \sum_{hk} \frac{\left( |F_{hk0}^{\text{exp}}| - |F_{hk0}^{\text{calc}}| \right)^2}{(\sigma_{hk0}^{\text{exp}})^2} \quad (6)$$

where the summation is over  $N$  measured diffraction peaks,  $\sigma_{hk0}^{\text{exp}}$  are the experimental errors in  $F_{hk0}^{\text{exp}}$  whereas  $F_{hk0}^{\text{calc}}$  are the structure factors of the trial structures.

The initial structures with the number of atoms in reconstructed unit cell varying between 134 and 140 were first tested for their stability in a reasonable range of substrate potentials and then the parameters  $U_L$ ,  $U_0$  and  $z_0$  were varied until the minimal  $\chi^2$  was reached. In this way we narrowed the possible initial structures to one, having 136 surface atoms in the reconstructed unit cell, shown in Fig. 3. This structure is very stable, it does not vary after random atomic displacements up to 0.286 Å and subsequent energy minimization. The variational parameters in the minimum of  $\chi^2$  ( $\chi^2 = 2.54$ ) are:  $U_0 = 0.28$  eV,  $U_L = 23$  and  $z_0 = 5.10$  Å. The average Sutton-Chen potential energy per adatom is  $E_{SC} = -3.045$  eV and the average adatom–substrate energy  $E_S = -0.230$  eV, giving  $E = -3.275$  eV for the average total potential energy per adatom.  $\chi^2$  varies by less than 10% for  $U_0$  varying between 0.16 and 0.70 eV.

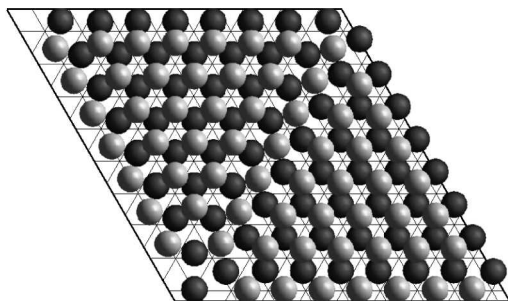


Fig. 3. The  $(3\sqrt{3} \times 3\sqrt{3})R30^\circ$  reconstructed unit cell with 136 atoms (73 in the lower and 63 in the upper plane) in the calculated model. The darker spheres represent the atoms in the lower plane. The underlying triangular net represents the periodicity of the simulated substrate potential which has minima in the centres of the triangles.

## 4 Results and Discussion

We would like to emphasize the strength of the present combined experimental-theoretical approach compared to the standard surface X-ray diffraction analysis based only on the Patterson-map analysis and  $\chi^2$  minimization [16].

The first advantage is related to the weakness of the standard method where the surface structure factors corresponding to the locations of the bulk contributions are not included in the Patterson analysis, thus leading to an incomplete Patterson map [10]. Omission of some peaks from the diffraction data can introduce errors in the final atomic positions. In Fig. 2 it is demonstrated that the peaks corresponding to  $(h, k) \equiv (0, 0) \pmod{9}$  have a dramatic effect: when they are omitted, the incomplete Patterson function shows 8 atoms along the reconstruction primitive vectors [Fig. 2(a)] instead of 9 that are retrieved if we complete the diffraction data with the model values [Fig. 2(b)]. In case of free FCC(111) stacked Al the lattice parameter is  $\sim 4\%$  larger than the corresponding sapphire distance. In the present case, the misfit is  $\sim 2 - 3\%$ , showing that the Al layer is strained by

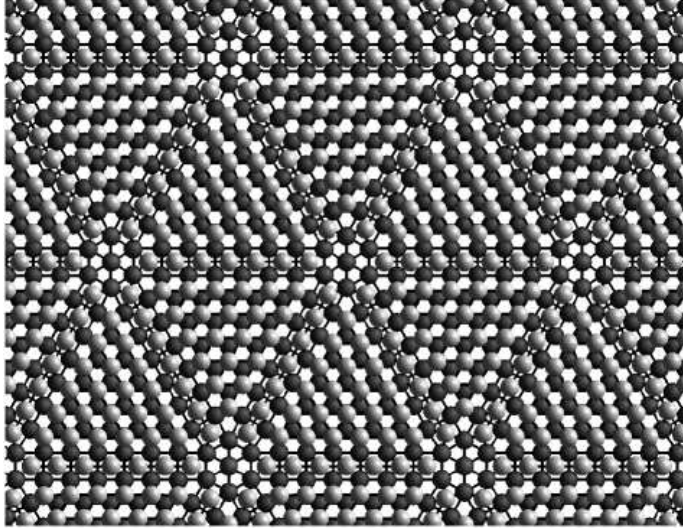


Fig. 4. The relaxed atomic configurations of the  $(3\sqrt{3} \times 3\sqrt{3})R30^\circ$  reconstruction. Clearly seen are the triangular domains with hexagonal [FCC(111)] structure separated by “walls” where the structure is FCC(001). At the corners of the triangles the density is lower.

the underlying sapphire lattice. Such overlayer yields significant intensities at the bulk peaks locations (corresponding to no expansion) as well as in the neighbouring peaks (12.5 % expansion). A standard analysis would thus favour the second components in the Al atom positions, hence probably over-estimating the expansion of the Al overlayer. The present approach avoids this effect because the bulk component is re-introduced via the interaction with the substrate, and thus the final structure would be closer to the real one than with the standard analysis.

The second advantage of the present method is that it yields a high-symmetry structure with negligible disorder which, we believe, is close to the “ideal” structure of the  $(3\sqrt{3} \times 3\sqrt{3})$  reconstruction while the experimental data correspond to a structure which may be substantially disordered.

The final, relaxed structure is shown in Fig. 4 and in Fig. 1 we compare the calculated (left-hand semi-circles) diffraction pattern with the experiment (right-hand semi-circles). Specific for this structure is a triangular pattern with the period  $3\sqrt{3}a_s$ . Inside these large triangles, the two Al planes are ordered hexagonally in FCC(111) planes. In the “down” triangle (upper left-hand side of Fig. 3) the lower-layer Al atoms are located in the centres of the underlying small up-triangles, representing the substrate potential, and the upper-layer atoms in the centres of the small down-triangles. In the “up” triangle (lower right-hand side of Fig. 3) the stacking is reversed. The two large triangles together, thus, form the rhombic reconstructed unit cell. Between the triangles, the lower-layer Al atoms are ordered in squares; together with the atoms in the upper layer they form semi-octahedra with an FCC(001) orientation. The semi-octahedral ordering is needed to compensate for the  $\sim 4\%$  lattice misfit between the sapphire substrate and the Al overlayer. In the corners of the large triangles we find small hexagonal vacancy islands where

several Al atoms are missing in the upper layer. The average density of the over-layer atoms is  $136/27 \approx 5$  Al atoms per unreconstructed surface unit cell and is surprisingly close to the density proposed for the  $(\sqrt{31} \times \sqrt{31})$  reconstruction [7]. In the large triangles, the nearest-neighbour Al-Al spacing of the lower layer is between 2.82 and 2.84 Å, giving a contraction of up to 1.5 % with respect to bulk Al. The spacing in the FCC(001) octahedra is similar, with a contraction of up to 2 %. In principle, our ground-state simulations predict a chiral structure with  $p6$  symmetry. The  $p6mm$  symmetry is restored either by superimposing both chiral orientations or by room-temperature thermal fluctuations since the deviations from the mirror symmetry are small, of the order 0.03 Å. It is interesting to note that the structure of the  $(3\sqrt{3} \times 3\sqrt{3})$  reconstruction, as proposed in this paper, is much less disordered than the final,  $(\sqrt{31} \times \sqrt{31})$  reconstruction [7,8].

The difference between the experimental and simulated diffraction patterns in Fig. 1 might have two origins. First, the adatom-adatom and the adatom-substrate potentials were treated in an approximate way, and second, there can be some disorder in the surfaces. Indeed, experimentally, the reconstruction with  $3\sqrt{3}$  symmetry can be prepared in very different states of order (as checked by electron or X-ray diffraction), depending on the exact annealing temperature and duration. A slight variation from the best conditions leads to a high level of background scattering as well as to different relative ratios of the structure factors. A minimization of  $\chi^2$  with respect to the Debye-Waller factor using the ROD program [16], for instance, and keeping all the atomic coordinates fixed improves the  $\chi^2$  value to  $\chi^2 = 2.05$ . The corresponding Debye-Waller factor increases to  $\sigma = 0.25$  Å, indicating that some kind of disorder (i.e., variation of the atomic structure between different reconstruction cells) is present on the prepared surface. In contrast, a standard minimization of  $\chi^2$  with the ROD program varying the atomic positions yields a much better agreement ( $\chi^2$  as low as 0.7!) but for very disordered and unphysical structures.

To conclude, on the basis of our GIXD experiments combined with the energy minimization using effective potentials, we propose a real-space structure of the  $(3\sqrt{3} \times 3\sqrt{3})$  reconstruction of  $\text{Al}_2\text{O}_3(0001)$ . We have shown that the combination of GIXD experiments with the simulations based on energy-minimization is a powerful tool to predict and understand the large unit cell reconstructions, in particular on oxides or insulators, where atomic-scale information from scanning force microscopy is still extremely scarce.

## Acknowledgement

I.V. would like to acknowledge the support of the UFR de Physique, Université Joseph Fourier in Grenoble and the hospitality of the Département de Recherche Fondamentale sur la Matière Condensée. The comments by Clemens Barth are gratefully acknowledged.

## References

- [1] P. Guénard, G. Renaud, A. Barbier and M. Gautier-Soyer, *Surface Rev. and Lett.* 5 (1997) 321.
- [2] R. Di Felice and J. E. Northrup, *Phys. Rev. B* 60 (1999) R16287.
- [3] A. Wander, B. Searle and N.M. Harrison, *Surf. Sci.* 458 (2000) 25.
- [4] T.M. French and G.A. Somorjai, *J. Phys. Chem.* 74 (1970) 2489.
- [5] G. Renaud, *Surf. Sci. Rep.* 32 (1998) 1.
- [6] G. Renaud, B. Villette, I. Vilfan and A. Bourret, *Phys. Rev. Lett.* 73 (1994) 1852.
- [7] I. Vilfan, F. Lançon and J. Villain, *Surf. Sci.* 392 (1997) 62.
- [8] C. Barth and M. Reichling, *Nature*, 414 (2001) 54.
- [9] G. Renaud, A. Barbier and M. Gautier-Soyer, unpublished.
- [10] W.S. Yang and R.G. Zhao, *Phys. Rev. Lett.* 56 (1986) 2877; J. Bohr, R. Feidenhans'l, M. Nielsen, M. Toney, R.L. Johnson and I.K. Robinson, *ibid.* 2878.
- [11] R. Baudoing-Savois, G. Renaud, M. De Santis, A. Barbier, O. Robach, P. Taunier, P. Jeantet, O. Ulrich, J.P. Roux, M.C. Saint-Lager, A. Barski, O. Geaymond, G. Berard, P. Dolle, M. Noblet and A. Mougin, *Nucl. Inst. and Meth. In Phys. Res. B.* 149 (1999) 213-227.
- [12] O. Robach, Y. Garreau, K. Aid and M.B. Veron-Jolliot, *J. Appl. Crystallography* 33 (2000) 1006.
- [13] A.P. Sutton and J. Chen, *Phil. Mag. Lett.* 61 (1990) 139.
- [14] M.W. Finnis and J.E. Sinclair, *Phil. Mag. A* 50 (1984) 45.
- [15] C. Verdozzi, D.R. Jennison, P.A. Schultz and M.P. Sears, *Phys. Rev. Lett.* 82 (1999) 799.
- [16] E. Vlieg, *J. Appl. Cryst.* 33 (2000) 401;  
[www.esfr.fr/computing/scientific/joint\\_projects/ANA-ROD/index.html](http://www.esfr.fr/computing/scientific/joint_projects/ANA-ROD/index.html).